Journal of Zhejiang University-SCIENCE A (Applied Physics & Engineering) *2024 25(8):631-649*
www.jzus.zju.edu.cn; www.springer.com/journal/11582
E-mail: jzus_a@zju.edu.cn

Research Article
https://doi.org/10.1631/jzus.A2300365

Gas film/regenerative composite cooling characteristics of the liquid oxygen/liquid methane (LOX/LCH4) rocket engine

Xinlin LIU, Jun SUN, Zhuohang JIANG, Qinglian LI✉, Peng CHENG, Jie SONG

Science and Technology on Scramjet Laboratory, College of Aerospace Science and Engineering, National University of Defense Technology, Changsha 410073, China

Abstract: The thermal protection of rocket engines is a crucial aspect of rocket engine design. In this paper, the gas film/regenerative composite cooling of the liquid oxygen/liquid methane (LOX/LCH4) rocket engine thrust chamber was investigated. A gas film/regenerative composite cooling model was developed based on the Grisson gas film cooling efficiency formula and the one-dimensional regenerative cooling model. The accuracy of the model was validated through experiments conducted on a 6 kg/s level gas film/regenerative composite cooling thrust chamber. Additionally, key parameters related to heat transfer performance were calculated. The results demonstrate that the model is sufficiently accurate to be used as a preliminary design tool. The temperature rise error of the coolant, when compared with the experimental results, was found to be less than 10%. Although the pressure drop error is relatively large, the calculated results still provide valuable guidance for heat transfer analysis. In addition, the performance of composite cooling is observed to be superior to regenerative cooling. Increasing the gas film flow rate results in higher cooling efficiency and a lower gas-side wall temperature. Furthermore, the position at which the gas film is introduced greatly impacts the cooling performance. The optimal introduction position for the gas film is determined when the film is introduced from a single row of holes. This optimal introduction position results in a more uniform wall temperature distribution and reduces the peak temperature. Lastly, it is observed that a double row of holes, when compared to a single row of holes, enhances the cooling effect in the superposition area of the gas film and further lowers the gas-side wall temperature. These results provide a basis for the design of gas film/regenerative composite cooling systems.

Key words: Liquid oxygen/liquid methane (LOX/LCH4) rocket engine; Gas film cooling; Regenerative cooling; Heat transfer characteristics

1 Introduction

In recent years, with the diversification and formalization of space missions, higher requirements have been placed on rocket engines in terms of their low cost, eco-friendliness, safety, and reliability. Liquid oxygen and methane propellants have received much attention for their ability to effectively lower launch costs, reduce pollution, and improve reliability (Trejo et al., 2016; Ruan et al., 2017; Zhang and Sun, 2020). The combination of liquid oxygen and methane in propellants has many advantages, such as a high specific impulse, good cooling performance, abundant resources, large storage space, and easily achievable multiple ignition and startup. Therefore, it has very broad application prospects in aerospace, especially in variable-thrust liquid rocket engines (Hong et al., 2019; Perakis and Haidn, 2020; Waxenegger-Wilfing et al., 2020).

The high-temperature and high-pressure gas of the engine thrust chamber can easily cause damage to the wall surface, so regenerative cooling is often used in engineering to avoid melting of the thrust chamber wall (Zhu and Liu, 2009; Gradl and Protz, 2020; Li et al., 2022; Yu et al., 2022). However, in the process of varying thrust, with the decrease of methane flow under low working conditions, the cooling capacity is greatly weakened and single regenerative cooling can hardly meet the thermal protection requirements of the engine (Zhang, 1984; Liang et al., 2021). The composite cooling scheme with film cooling can further improve the cooling capacity and significantly reduce

✉ Qinglian LI, peakdreamer@163.com
Xinlin LIU, https://orcid.org/0000-0001-7439-854X

Received July 16, 2023; Revision accepted Oct. 24, 2023;
Crosschecked Apr. 19, 2024; Online first June 11, 2024

the wall heat flow and temperature. It is of great significance for the thermal protection of the engine thrust chamber (Gao et al., 2018; Wan et al., 2020).

According to the state of the film, film/regenerative composite cooling can be divided into gas film/regenerative composite cooling and liquid film/regenerative composite cooling. The wall temperature of the thrust chamber is usually high at the head of the combustion chamber and the convergent section of the nozzle. For the high-temperature area, single regenerative cooling has difficulty in meeting the cooling requirements, and film cooling needs to be introduced as an auxiliary to enhance the cooling effect.

Liquid film/regenerative composite cooling is adopted in liquid rocket engines, and involves injecting liquid propellant onto the combustion chamber inner wall to form a liquid film. The thermal protection of the thrust chamber is achieved by using liquid film evaporation and a dissipated gas film. Currently, liquid film/regenerative composite cooling has been widely applied to a series of liquid oxygen/kerosene engines. The RD-170 and RD-171 engines, used in the "Energia" launch vehicle of the former Soviet Union, employ a liquid film/regenerative composite cooling scheme to maintain a wall temperature below 773 K. The YF-100 is a liquid oxygen/kerosene engine developed in China which also adopts liquid film/regenerative composite cooling (Sun and Zhang, 2016). Researchers have also conducted extensive research on liquid film/regenerative composite cooling. Zhang et al. (2007) conducted numerical simulations to investigate liquid film/regenerative composite cooling and successfully calculated the coupled heat transfer between the high-temperature gas, liquid film, wall surface, and regenerative coolant. Sun et al. (2013) solved the Navier-Stokes (N-S) equation in the liquid/gas film region and the regenerative coolant region, calculating the results under each flow field parameter. Yang and Sun (2013) derived the calculation method of liquid film length and thickness through consideration of evaporation, entrainment, convection, heat conduction, radiation, and other factors, and analyzed the influence of liquid film flow on heat transfer characteristics.

Gas film cooling is a method used to protect the downstream high-temperature regions by introducing gas from disscrete holes or slots on the wall (Metzger et al., 1968; Goldstein, 1971). Gas film cooling can not only achieve active wall cooling, but it also reduces drag and blows away the boundary layer (Cary and Hefner, 1972). Gas film cooling was initially used for de-icing of aircraft wings and was later applied to the cooling of gas turbine blades. It was also used for wall cooling in the nozzle divergent section of rocket engines (Keller and Kloker, 2017). The F-1 engine of the US "Saturn V" launch vehicle used radial holes to inject turbine exhaust gas (at about 673 K) for gas film cooling (Sun and Zhang, 2016). However, gas film/regenerative composite cooling technology is currently mainly used to cool the combustion chamber wall of scramjet engines. Research now mainly focuses on gas film flow characteristics and heat transfer characteristics.

Goldstein et al. (1966) initiated research on supersonic film cooling. They conducted experiments in a continuous wind tunnel under Mach number Ma=3 conditions to investigate various film cooling techniques. The results demonstrated that supersonic film cooling provides superior cooling efficiency compared with subsonic film cooling. Lushchik and Yakubenko (2001) predicted, based on a numerical simulation, the cooling effectiveness and friction coefficient distribution in engine nozzle film cooling. Using numerical simulation, Yang et al. (2003, 2005) conducted studies on the cooling mechanism of gas film under laminar and turbulent conditions. They also established models for gas film cooling in laminar and turbulent boundary layers. Heufer and Olivier (2006) and Keller et al. (2015) conducted research on film cooling under supersonic conditions based on both experiment and simulation. The results demonstrated that the effectiveness of film cooling is greatly influenced by the density, specific heat, and other physical properties of the film coolant. Konopka et al. (2012) conducted a study on the interaction between shock waves and supersonic film using the large-eddy simulation (LES) method. The research results indicated that, when shock waves act on the boundary layer, the resulting flow separation region is relatively small and the impact on film cooling is also minimal. Howard and Srokowski (1977) investigated the effects of the jet slot on cooling and drag reduction under Ma=6 through experimental research. The results showed that the more the jet slots and the longer the gas film, the better the cooling effect. However, a single slot had the best drag reduction effect. Keller and Kloker (2017) conducted a study on the impact of the film coolant's physical properties and the boundary layer state on the heat transfer characteristics

of film cooling based on the direct numerical simulation (DNS) method. The film cooling was achieved by injecting coolant through a 90° inclined slot in a direction perpendicular to the main flow. Peng and Jiang (2009) and Peng et al. (2017) analyzed the influence of flow parameters and structural parameters on the efficiency of film cooling based on numerical simulation.

Much research has also been conducted on the heat transfer characteristics of film cooling. Dannenberg (1962) conducted experimental research on supersonic film cooling with a mainstream Mach number of 10. The results indicated that supersonic film cooling exhibits a favorable cooling effect. Kanda et al. (1994) established a gas film cooling model based on the experimental results of a compressible mixed layer and the analytical results of a turbulent boundary layer. These were combined with a quasi-one-dimensional regenerative cooling model of the scramjet to establish a one-dimensional gas film/regenerative composite cooling model. Takita and Masuya (2000) performed a numerical simulation study on hydrogen film cooling, considering the chemical reaction between hydrogen and oxygen. The results indicated that the impact of the chemical reaction on film cooling was minimal and was mainly attributed to a significant separation distance between the flame generated by film combustion and the wall, as well as to the relatively low heat release from the flame. Heufer and Olivier (2006) conducted a comprehensive investigation on the transverse film cooling of wedge-shaped bodies in hypersonic mainstream flows using a combination of experimental and numerical simulation approaches. The results demonstrated that film cooling in hypersonic flows significantly mitigates the thermal load on the body, thus making it a highly effective thermal protection technique. Zhang SL et al. (2016) proposed a gas film/regenerative composite cooling scheme for multi-effect utilization of hydrocarbon fuel cooling capacity and preliminarily verified its feasibility through experiments. Zuo et al. (2018) developed a quasi-one-dimensional model for gas film/regenerative composite cooling of scramjet engines; experimental validation was conducted to ensure its accuracy. Based on this model, a further simulation study was performed to investigate the influence of cooling parameters on the cooling performance.

In the liquid oxygen/methane expander cycle engine, liquid methane typically undergoes a phase change to gas after passing through the regenerative cooling channel (RCC). Thus, the combination of gas film cooling and regenerative cooling can be employed to further enhance the thermal protection capability of the thrust chamber (Song et al., 2021). Although there have been some studies on gas film/regenerative composite cooling, most studies are based on scramjet engines. Few focus on the heat transfer characteristics and influencing factors of the gas film/regenerative composite cooling of liquid oxygen/liquid methane (LOX/LCH4) engines, which need further exploration.

The electric expander cycle liquid rocket engine (EEC) is a new type of liquid oxygen/methane variable-thrust rocket engine in its early stages (Liang et al., 2021). As shown in Fig. 1, the EEC combines the expansion cycle engine with the electric pump cycle engine. Liquid methane is pressurized by the electric pump, flows through the regenerative cooling channel in the thrust chamber, absorbs heat, and undergoes phase change. The gaseous coolant drives the turbine to produce power and then the turbine drives the centrifugal pump to pressurize the liquid oxygen.

This study aims to explore the flow heat transfer characteristics of the gas film/regenerative composite cooling of LOX/LCH4 engines to reveal the influence of cooling system parameters on cooling performance and thereby improve the composite cooling efficiency. Based on LOX/LCH4 electric expander cycle engines, a one-dimensional heat transfer calculation model of gas film/regenerative composite cooling is established. The model is verified by comparing the calculated results with the hot test results of the LOX/LCH4 engine. In addition, the influence law of the gas film flow ratio and introduction position on the cooling characteristics is analyzed. The research results can provide a reference for the design of a gas film/regenerative composite cooling scheme of liquid rocket engine.

2 Input parameters and calculation model

2.1 Physical model

Table 1 illustrates the technical metrics of the thrust chamber. The propellant combination selected is LOX/LCH4, and the cooling scheme adopts a gas film/regenerative composite cooling with methane as the coolant. The design pressure ($p_{c,max}$) of the combustion chamber under 100% rated power level (RPL) is 3 MPa, the mixing ratio (MR) is 3.2, and the total

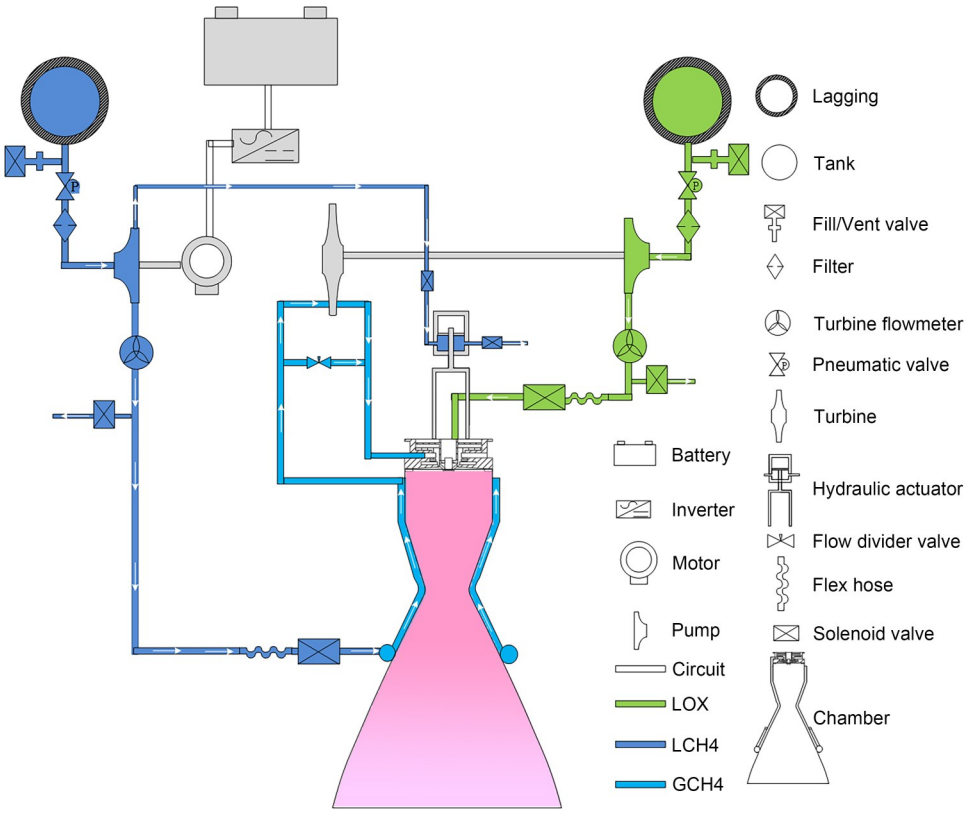

Fig. 1 Electric expander cycle system scheme. GCH4: gas methane. Reprinted from (Liang et al., 2021), Copyright 2021, with permission from Elsevier. References to color refer to the online version of this figure

Table 1 Technical metrics of the thrust chamber

Parameter	Value
Design pressure, $p_{c,max}$ (MPa)	3
Mixing ratio (MR)	3.2
Expansion ratio, ε	4
Throat radius, R_t (mm)	32.3
Total flow rate of propellant, $\dot{m}_p$ (kg/s)	5.67

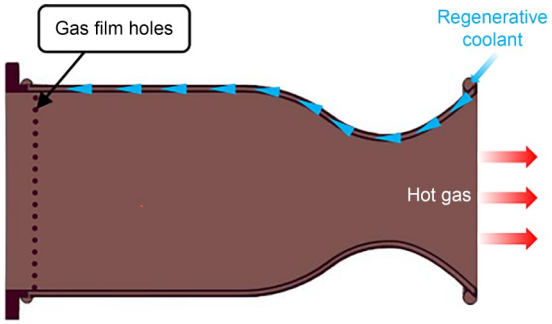

Fig. 2 Engine thrust chamber model

flow rate of propellant ($\dot{m}_p$) is 5.67 kg/s. The expansion ratio (ε) is 4, the throat radius (R_t) is 32.3 mm, and the length of the thrust chamber cylinder is 150 mm. Fig. 2 shows the thrust chamber configuration and direction of methane flow. In the gas film/regenerative composite cooling scheme, the regenerative coolant enters the cooling channel from the position where the nozzle expansion ratio is 4.

The gas film/regenerative composite cooling scheme, as proposed in this paper, uses liquid methane as the coolant as shown in Fig. 2. The coolant flows from the liquid collection cavity at the thrust chamber outlet into the regenerative cooling channel inside the thrust chamber. During this passage through the cooling channel, the coolant absorbs heat and undergoes a phase change. Upon reaching the exit of the cooling channel, the coolant has completely transitioned into the gaseous state. Then a portion of the gaseous coolant is directly introduced onto the thrust chamber inner wall to facilitate film cooling, while the remaining coolant is injected into the combustion chamber to serve as fuel for combustion (Li et al., 2022).

For the gas film/regenerative composite cooling scheme, complex flow, combustion, and heat transfer processes occur near the thrust chamber wall. The thrust

chamber thermal protection process primarily involves convective heat transfer, thermal conduction, and radiative heat transfer. Inside the thrust chamber, the gas film acts as a barrier, separating the high-temperature gas from the thrust chamber wall while absorbing some heat through its own flow. This leads to changes in the boundary layer structure on the thrust chamber inner wall, thereby affecting convective heat transfer between the inner wall and the high-temperature gas. As a result, the convective heat transfer coefficient on the gas side of the thrust chamber wall decreases. Heat is transferred from the gas to the gas-side wall through convection and thermal radiation. The gas-side wall exhibits a higher temperature and the heat on the gas-side wall is conducted to the coolant-side wall through thermal conduction. Finally, the heat on the coolant-side wall is dissipated through convective heat transfer from the coolant, thereby achieving effective thermal protection for the thrust chamber.

The number of regenerative cooling channels (N) of variable rectangular cross-section is 84, and the channels have a gradually shrinking and expanding structure (Pizzarelli et al., 2014). That is, along the coolant flow direction, the width of the cooling channel groove (a) gradually decreases from 1.5 mm at the entrance to 1 mm at the throat. After passing through the throat, it gradually increases along the convergent segment, until the cylinder segment recovers to 1.5 mm. The rib width (b) changes with the groove width. Table 2 and Fig. 3 show the specific parameters including the groove height (H) and wall thickness (δ_w). The gas film coolant is injected to the inner wall through discrete round holes, with apertures of 1.5 mm, which are uniformly distributed on the thrust chamber wall.

Table 2 Geometric dimensions of the cooling channel

Item	a (mm)	b (mm)	H (mm)	δ_w (mm)
Cylinder section	1.5	3.4	3.0	1.0
Nozzle throat	1.0	1.5	3.0	1.0
Inlet of RCC	1.5	3.4	3.0	1.0

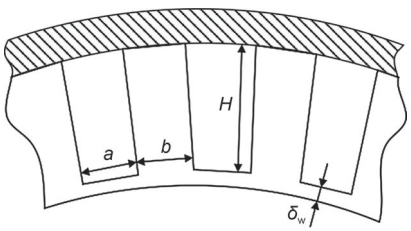

Fig. 3 Schematic diagram of the cooling channel structure

As shown in Fig. 3, the inner wall of the thrust chamber is made of chromium-zirconium copper alloy (CuCrZr), and the outer wall of the thrust chamber is made of high-temperature alloy (GH3536) with a thickness of 2 mm. The relevant parameters of the materials for the inner and outer walls are shown in Table 3. Due to the difference in materials between the inner and outer walls, a diffusion welding method is used here to weld the inner and outer walls together.

Table 3 Alloy performance parameters

Material	Thermal conductivity (W/(m^2·K))	Limit temperature (K)
Chromium-zirconium copper alloy (CuCrZr)	343	823
High-temperature alloy (GH3536)	33	1400

2.2 Calculation model

To simplify the calculations, this paper makes the following assumptions:

(1) The gas has been evenly mixed at the entrance and the gas is ideally non-viscous. The internal degrees of freedom are in equilibrium, and the flow process is isentropic. In aerodynamics, it is common to calculate the flow parameters at different positions inside a Laval nozzle based on the isentropic relation (Zeng et al., 2016). Similarly, it is assumed here that the flow inside the nozzle is also isentropic. Taking reference from the simulation for liquid film/regenerative composite cooling of the liquid oxygen/kerosene thrust chamber, it is considered that the combustion process is completed at the inlet of the thrust chamber. The distribution of gas parameters inside the combustion chamber is assumed to be uniform and in a state of thermodynamic equilibrium (Yang and Sun, 2013).

(2) The chemical reaction between gas film and mainstream gas is ignored. Referring to previous research (Takita and Masuya, 2000) on hydrogen gas film cooling, it can be observed that the flame generated by gas film combustion is generally far away from the wall and the heat release from the flame is limited. Therefore, the chemical reactions between the gas film and the mainstream have little effect on gas film cooling, so it can be assumed that the chemical reactions between the gas film and the mainstream can be neglected.

(3) Axial heat conduction in the wall surface is ignored. Referring to the one-dimensional heat transfer calculation model for a scramjet engine, the axial heat conduction process on the thrust chamber wall is neglected in this study (Miao et al., 2020a, 2020b).

(4) Heat transfer between the thrust outdoor wall and the external environment is ignored. Due to the small temperature difference between the outer wall and the environment, it can be assumed that there is negligible heat exchange between the outer wall and the environment. This simplifying assumption has also been used in the simualtion studies conducted on liquid oxygen/methane regenerative cooling (Song et al., 2021) and on liquid oxygen/kerosene liquid film/regenerative composite cooling (Yang and Sun, 2013).

2.2.1 Regenerative cooling model

2.2.1.1 Calculation of heat flux

Based on the above assumptions, the heat transfer process in the thrust chamber mainly includes the following parts: heat transfer from high-temperature gas film to the gas-side wall, heat transfer from the gas-side wall to the coolant-side wall, heat transfer from the coolant-side wall to the regenerative coolant, and heat removed by the regenerative coolant, as shown in Fig. S1 of the electronic supplementary materials (ESM). According to Fourier's law (Huzel and Huang, 1992; Hao et al., 2021), the heat flux density (q) in the heat transfer process can be calculated by

$$q=\frac{T_{\mathrm{aw}}-T_{\mathrm{f}}}{\frac{1}{h_{\mathrm{g}}}+\frac{\delta_{\mathrm{w}}}{\lambda_{\mathrm{w}}}+\frac{1}{h_{\mathrm{co}}}}, \tag{1}$$

where T_{aw} is the gas-side adiabatic wall temperature, T_{f} is the coolant temperature, and the subscript 'f' represents the coolant parameter. λ_{w} is the heat transfer coefficient of the thrust chamber wall. h_{g} and h_{co} are respectively gas-side and coolant-side total convective heat transfer coefficients.

The expression for h_{co} is as follows:

$$h_{\mathrm{co}}=\frac{h_{\mathrm{f}}\eta_0 S_{\mathrm{tot}}}{S_{\mathrm{g}}}, \tag{2}$$

where h_{f} represents the coolant-side convective heat transfer coefficient, and η_0 represents the total efficiency of rib surface. S_{tot} represents the total rib surface area, and is given by $S_{\mathrm{tot}}=S_1+S_2$, where S_1 and S_2 correspond to the bottom and side surface areas of the cooling channel, respectively, as shown in Fig. S1. Furthermore, S_{g} represents the total surface area of the gas-side wall, also shown in Fig. S1.

2.2.1.2 Calculation of convective heat transfer coefficient on the gas side

The convective heat transfer coefficient h_{g} on the gas side is calculated by the semi-empirical Bartz formula (Huzel and Huang, 1992; Pizzarelli, 2021). The specific expression for h_{g} is detailed in Section S2 of the ESM.

2.2.1.3 Calculation of the convective heat transfer coefficient on the regenerative coolant side

Using the coolant Nusselt number (Nu_{f}), the regenerative coolant-side heat transfer coefficient (h_{f}) can be calculated by distinguishing the phase and flow state (Jagannathan et al., 2018; Phu and Hap, 2020; Ali et al., 2021):

$$h_{\mathrm{f}}=\frac{Nu_{\mathrm{f}}\lambda_{\mathrm{f}}}{D_{\mathrm{h}}}, \tag{3}$$

where λ_{f} and D_{h} represent the coolant thermal conductivity and the hydraulic diameter, respectively. When the regenerative coolant is in the liquid laminar flow zone, Nu_{f} can be calculated according to the Zider-Taylor equation (Bertsch et al., 2008):

$$Nu_{\mathrm{f}}=1.86\left(\frac{Re_{\mathrm{f}}Pr_{\mathrm{f}}}{\frac{L}{D_{\mathrm{h}}}}\right)^{\frac{1}{3}}, \tag{4}$$

where L is the cooling channel length. Pr_{f} and Re_{f} are the coolant Prandtl number and Reynolds number, respectively. When the regenerative coolant is in the liquid turbulent region or the gas phase, it can be calculated according to the Gnielinski formula (Thome and Consolini, 2010):

$$Nu_{\mathrm{f}}=\frac{\frac{f}{8}\times(Re_{\mathrm{f}}-1000)Pr_{\mathrm{f}}}{1+12.7\sqrt{\frac{f}{8}}\left(Pr_{\mathrm{f}}^{\frac{2}{3}}-1\right)}. \tag{5}$$

The coefficient of friction f in Eq. (5) can be expressed as

$$f=\left(1.82\log\left(Re_{\mathrm{f}}\right)-1.64\right)^{-2}. \tag{6}$$

When the coolant is in the two phases, the convective heat transfer coefficient can be calculated using the micro-channel liquid nitrogen flow boiling heat transfer correlation obtained by our team (Zhang et al., 2020). It is worth noting that although the correlation used here is for low-temperature liquid nitrogen, the variables in the correlation are dimensionless. Therefore, the empirical correlation for low-temperature liquid nitrogen used here is also applicable to the heat transfer calculation model for low-temperature liquid methane (Song et al., 2021; Liang et al., 2023).

$$Nu_{\mathrm{f}}=\begin{cases}12.46Bo^{0.544}We^{0.035}K_{\mathrm{p}}^{0.614}X^{0.031}, & x_{\mathrm{f}}<0.6,\\ 0.00136Bo^{-1.442}We^{0.074}, & x_{\mathrm{f}}\geqslant 0.6,\end{cases} \tag{7}$$

where Bo, We, and X are the boiling number, Weber number, and Martinelli number, respectively, K_{p} is the dimensionless pressure parameter, and x_{f} is the coolant dryness. The dimensionless parameters shown in Eq. (7) can be expressed as in Section S3 of the ESM.

2.2.2 Pressure drop model

The pressure drop in RCC (Δp_{rc}) can be divided into four parts: frictional pressure drop Δp_{fr}, local pressure drop Δp_{lo}, gravity pressure drop Δp_{gr}, and acceleration pressure drop Δp_{ac} (Gururatana et al., 2021).

$$\Delta p_{\mathrm{rc}}=\Delta p_{\mathrm{fr}}+\Delta p_{\mathrm{lo}}+\Delta p_{\mathrm{gr}}+\Delta p_{\mathrm{ac}}, \tag{8}$$

where Δp_{lo} and Δp_{gr} are ignored when calculating the pressure drop (Song et al., 2021). The specific expressions for Δp_{fr} and Δp_{ac} are detailed in Section S4 of the ESM.

2.2.3 Gas film cooling model

2.2.3.1 Calculation of the gas film cooling efficiency

The gas film cooling efficiency η can be calculated using the Grisson gas film cooling efficiency formula (Zhang ZL et al., 2016):

$$\eta=\left\{1+\frac{c_{p,\mathrm{g}}}{c_{p,\mathrm{gf}}}\left[0.325\left(Z_{\mathrm{gf}}+Z_{\mathrm{gf0}}\right)^{0.8}-1\right]\right\}^{-1}, \tag{9}$$

where $c_{p,\mathrm{g}}$ is the mainstream gas specific heat capacity at constant pressure, and $c_{p,\mathrm{gf}}$ is the gas film specific heat capacity at constant pressure. The non-dimensional distance downstream of the cooling film Z_{gf} and the non-dimensional location of the cooling film effective leading edge Z_{gf0} can be calculated as follows:

$$Z_{\mathrm{gf}}=G_{\mathrm{g}}\mu_{\mathrm{g}}^{0.25}\left(\frac{\dot{m}_{\mathrm{f}}}{\pi D_{\mathrm{c}}}\right)^{-1.25}z_{\mathrm{gf}}, \tag{10}$$

$$Z_{\mathrm{gf0}}=\left(3.08+Z_{\mathrm{gf}}{}^{0.8}\right)^{1.25}-Z_{\mathrm{gf}}, \tag{11}$$

where G_{g} is the gas mass flow rate, μ_{g} is the gas dynamic viscosity, $\dot{m}_{\mathrm{f}}$ is the coolant mass flow rate, D_{c} is the diameter of the thrust chamber along the axis, and z_{gf} is the downstream distance from the starting point of the gas film.

2.2.3.2 Calculation of the adiabatic wall temperature

In terms of cooling efficiency, the adiabatic wall temperature T_{aw} (Li et al., 2022) in composite cooling can be defined as:

$$T_{\mathrm{aw}}=T_{\mathrm{g}}-\eta\left(T_{\mathrm{g}}-T_{0}\right), \tag{12}$$

where T_{g} and T_0 are the mainstream gas temperature and initial cooling film temperature, respectively. The meaning of T_{aw} is the same as the meaning of the gas-side adiabatic wall temperature mentioned in Eq. (1).

2.3 Input parameters

As the cooling capacity of the electric expander cycle engine is insufficient at low working conditions and considering the previous analysis, the heat transfer calculation and analysis of the gas film/regenerative composite cooling characteristics were carried out under 75% working conditions. The specific input parameters are shown in Table 4, where T_{c} and p_{c} are the combustion temperature and pressure, respectively, M is the gas molar mass, γ is the combustion chamber gas specific heat ratio, and $T_{\mathrm{rc,i}}$ and $p_{\mathrm{rc,i}}$ are the inlet temperature and pressure of coolant, respectively. Among them, the thermodynamic parameters of the coolant methane and mainstream gas are obtained by thermal calculation software. It should be noted that when part of methane is allocated for gas film cooling, the mixing ratio of the mainstream gas will change and the parameters of the mainstream gas will need to be recalculated.

2.4 Calculation process

The differential method is adopted to carry out the heat transfer calculation of composite cooling. As

Table 4 Input parameters of the heat transfer calculation

Parameter	Value
p_c (MPa)	2.25
T_c (K)	3381
γ	1.128
M (g/mol)	20.8
$\dot{m}_f$ (kg/s)	1.01
$T_{rc,i}$ (K)	125
$p_{rc,i}$ (MPa)	4.116

shown in Fig. 4, the thrust chamber is evenly divided into n units along the axis (n=400), and then the regenerative cooling channels are evenly divided into n units along the axis. The outlet temperature of the regenerative cooling channel, namely the initial temperature of the gas film, is assumed as T_0. According to the input parameters and calculation model, the cooling efficiency, adiabatic wall temperature, heat flux density, and other related parameters of each node are calculated successively. Finally, the calculated coolant temperature at the cooling channel unit outlet is obtained. The cycle is iterated until the relative error between the assumed value and the calculated value is less than 10^{-6} when the calculation is stopped. Fig. 5 shows the detailed calculation process.

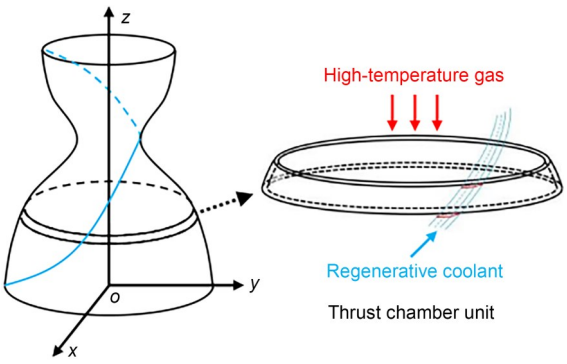

Fig. 4 Schematic diagram of the thrust chamber unit

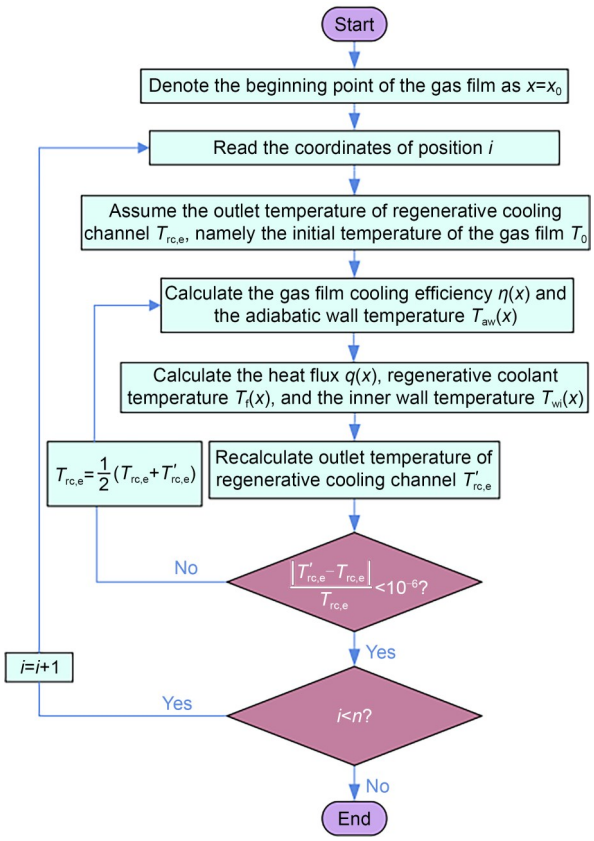

Fig. 5 Heat transfer calculation flow chart

3 Calculation results and analysis

3.1 Model validation

To validate the accuracy of the computational model, a hot test was carried out on the 6 kg/s level gas film/regenerative composite cooling thrust chamber. The test system is shown in Fig. 6. Under the driving force of high-pressure nitrogen, methane sequentially flows through the Venturi tube, solenoid valve, and cooling channels of the thrust chamber. It finally enters the combustion chamber through the top cover ring gap injection. Similarly, liquid oxygen, driven by high-pressure nitrogen, passes through the Venturi tube and solenoid valve, and enters the combustion chamber through the pintle injector. The combustion of methane and liquid oxygen inside the thrust chamber produces high-temperature and high-pressure combustion gases, generating thrust. Pre-cooling valves for liquid oxygen and liquid methane are positioned upstream of the main valves, serving the purpose of pre-cooling and shut-down purging. Additionally, temperature and pressure measurement points are placed at the inlet and outlet of the cooling channels to obtain heat transfer characteristic parameters.

The geometric characteristics of the composite cooling thrust chamber, excluding the length of the cylindrical section, remain consistent with those described in Section 2.1 for the 6 kg/s level thrust chamber. The thrust chamber is manufactured adopting additive manufacturing techniques. The thrust chamber wall material

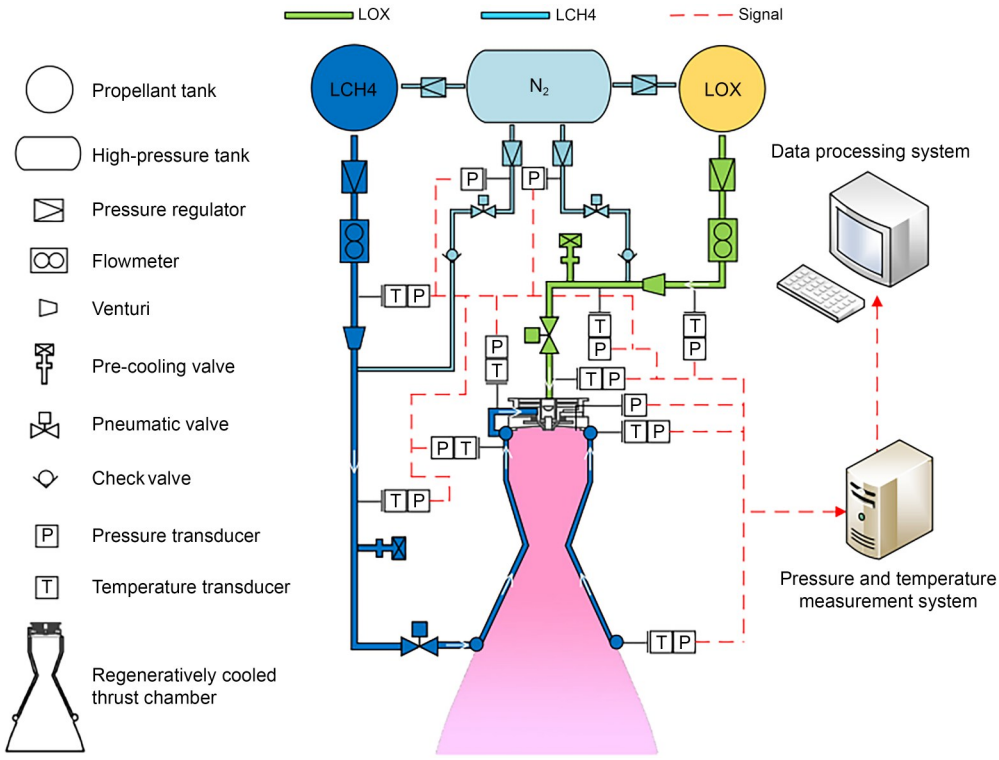

Fig. 6 Schematic diagram of the composite cooling thrust chamber hot test system. References to color refer to the online version of this figure

is composed of high-temperature alloy (GH3536), with an inner wall thickness of 0.6 mm, and the relevant parameters of the high-temperature alloy are shown in Table 3. The thermal protection of the thrust chamber is achieved through a combination of regenerative cooling and gas film. Gas film is implemented using three rows of holes, situated at the head of the thrust chamber, the beginning of the convergent section, and 45 mm downstream from the convergent section, as illustrated in Fig. 7. The gas film flow rate is 20% of the total methane flow rate. The regenerative cooling channel features a gradually shrinking and expanding structure, with specific dimensions provided in Table 5.

The experimental conditions are presented in Table 6. The thrust chamber hot test scene is shown in Fig. 8. The calculation model takes into account the combustion chamber temperature T_c and pressure p_c, as well as the coolant inlet temperature $T_{rc,i}$ and pressure $p_{rc,i}$ as input parameters. The model calculates the heat transfer characteristic parameters along the regenerative cooling channel for different experimental conditions. The calculation results are then compared with the experimental data, as in Fig. 9. The comparison reveals that the error in predicting the coolant temperature

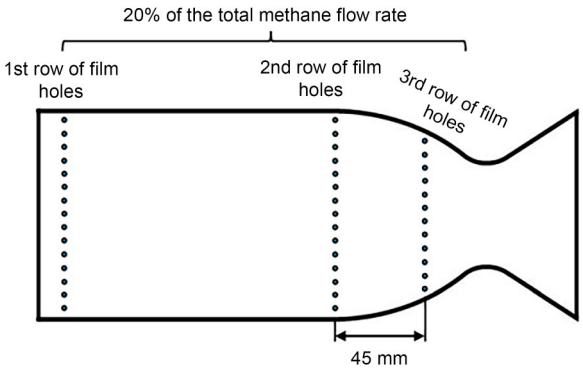

Fig. 7 Diagram of gas film injection point

rise is less than 10%, while the error in predicting the coolant pressure drop is approximately 25%. The model demonstrates good accuracy in predicting temperature, although slightly lower accuracy in predicting pressure. The pressure drop is influenced by factors such as processing errors in additive manufacturing and the gas film introduction holes, which affect the flow of the coolant. As a result, there is a relatively large error in predicting the pressure drop. However, the calculation results still provide the meaningful information regarding the general trends of coolant pressure drop

Table 5 Cooling channel dimension parameters

Position	Groove width (mm)	Rib width (mm)	Groove height (mm)	Number of grooves
Cooling channel inlet	3.3	1.7	2.0	82
Throat	1.0	1.5	2.0	82
Cooling channel outlet	2.8	2.2	2.0	82

Table 6 Experimental measurement parameters

Experiment	p_c (MPa)	MR	$\dot{m}_f$ (kg/s)	$p_{rc,i}$ (MPa)	$T_{rc,i}$ (K)
Experiment-1	2.71	3.18	1.29	5.59	141.3
Experiment-2	2.84	3.25	1.32	5.64	135.7
Experiment-3	2.81	3.29	1.27	5.15	137.9

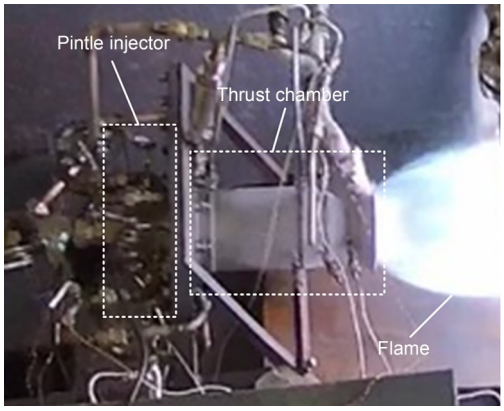

Fig. 8 Thrust chamber hot test

within the thrust chamber cooling channels, which is essential for heat transfer analysis.

It is worth mentioning that the thrust chamber used in the experiment is an initial design intended for model validation. At the time, the heat transfer calculation model was still under development and lacked accurate validation. Consequently, the design process of this thrust chamber did not undergo meticulous simulation calculations. However, through thermal tests conducted on this thrust chamber, the accuracy of the heat transfer model could be verified, thereby providing a foundation for optimizing the thrust chamber's design. The thrust chamber mentioned in Fig. 2 represents an enhanced design based on the thrust chamber employed in the experiment. Hence, there exists a slight disparity between the thrust chamber used in the experiment and the one employed in the simulation.

3.2 Influence of the gas film flow rate on the composite cooling performance

In this study, the heat transfer characteristic parameters are calculated when the gas film mass flow rates are 10%, 15%, 20%, and 25% that of methane. They are then compared with the regenerative cooling parameters to analyze the influence of the gas film flow rate on the cooling performance. Table S1 of the ESM shows the detailed parameters of the four schemes.

It should be noted that in the transient processes of an engine, the heat transfer in the engine system has not yet reached a steady state. The wall temperature of the thrust chamber is continuously increasing during this period. Typically, the peak wall temperature of the thrust chamber during the transient phase is lower than that during the steady-state phase. This observation is also supported by previous simulation results on the dynamics of propulsion systems (Zhou et al., 2021).

In the thermal protection design and research of the thrust chamber, the maximum wall temperature is of particular interest to researchers. Therefore, the focus of this study is the heat transfer characteristics of the thrust chamber under steady-state conditions. The results of the calculations for the heat transfer characteristics of composite cooling are also results under the steady-state condition.

3.2.1 Film cooling efficiency

Fig. 10 shows the changes in the cooling efficiency along the axial direction of the thrust chamber under different gas film flow rates. The four efficiency distribution curves have the same variation trend. Along the gas film flow direction, the cooling efficiency remains unchanged in the initial region, known as the gas film core region (Konopka et al., 2012). Upon mixing the gas film and mainstream gas, the temperature of the gas film increases gradually and the cooling efficiency decreases exponentially. The cooling efficiency remains above 10% until reaching the nozzle exit. This shows that the protective effect of the gas film injected from the head of the thrust chamber on the wall can be extended to the nozzle outlet. The gas film flow rate has a significant impact on the cooling efficiency. The higher the gas film mass flow rate, the higher the cooling efficiency at the same position. When

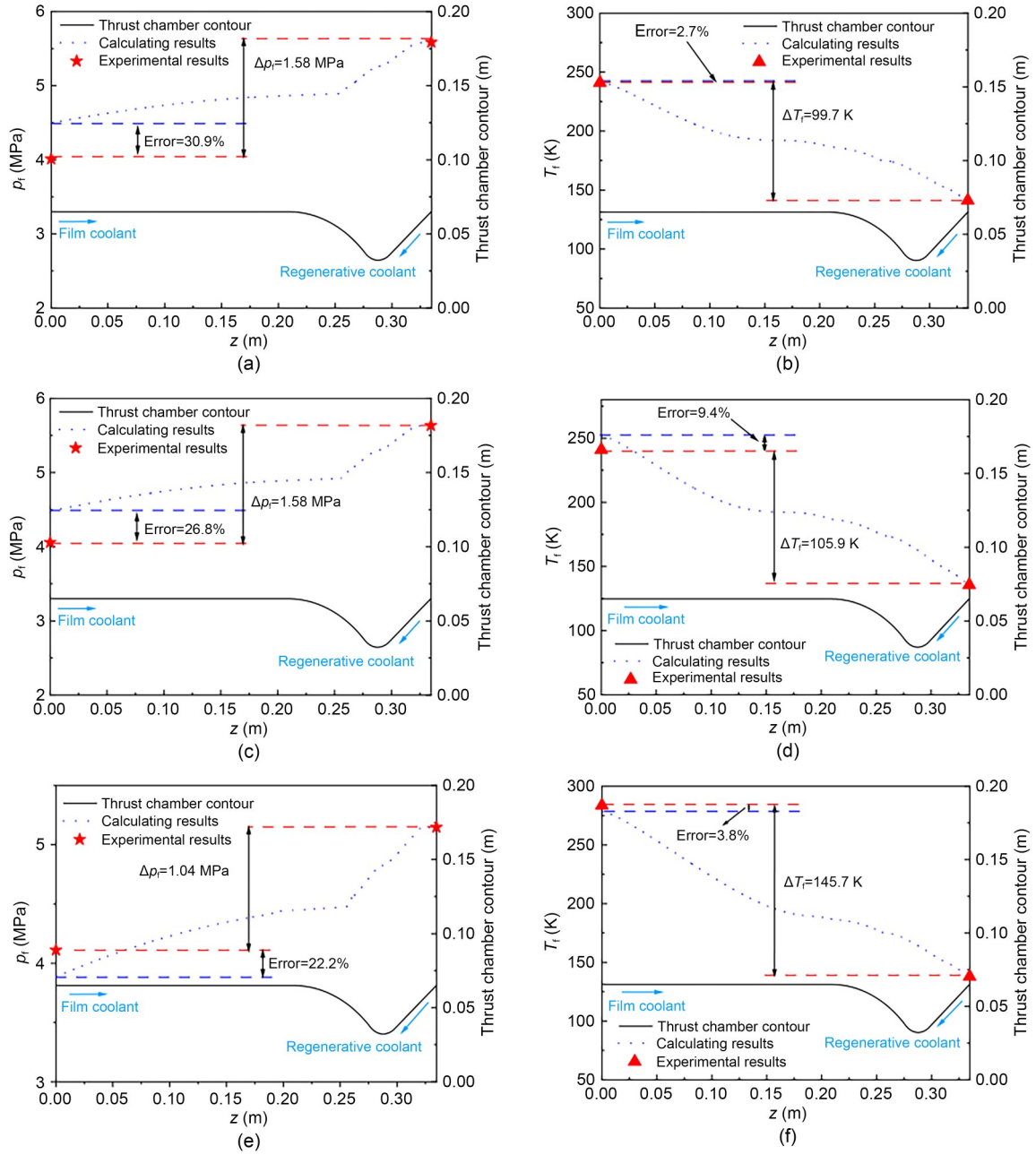

Fig. 9 Comparison between calculation results and experimental results: (a) coolant pressure (p_f) of Experiment-1; (b) coolant temperature of Experiment-1; (c) coolant pressure of Experiment-2; (d) coolant temperature of Experiment-2; (e) coolant pressure of Experiment-3; (f) coolant temperature of Experiment-3

the gas film flow rate is 10%, the cooling efficiency at the nozzle outlet is only 13%, increasing to 22% when the gas film flow rate is 20%. This is because a higher mass flow rate allows the gas film to absorb more heat, resulting in more effective heat transfer. Therefore, when considering only the cooling effect, a higher proportion of the gas film mass flow leads to an improved cooling effect.

3.2.2 Temperature, pressure, and dryness of the regenerative coolant

Fig. 11a shows the distribution of the dryness of the regenerative coolant along the axial direction of the thrust chamber. Along the flow direction of the regenerative coolant, liquid methane undergoes an endothermic phase transition in the cooling channel,

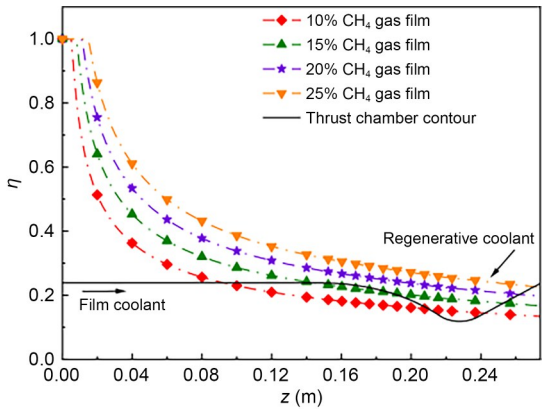

Fig. 10 Distribution of gas film cooling efficiency

successively undergoing three phases: the liquid-phase, two-phase, and gas-phase. The two-phase region can be further divided into the enhanced heat transfer region ($0<x<0.6$) and the heat transfer deterioration region ($0.6\leqslant x<1$). Meanwhile, it should be noted that the boundary may be just a reference and is only a probable value determined by most experimental data. With the increase of the gas film flow rate, the phase turning point of the regenerative coolant gradually moves toward the outlet of the regenerative cooling channel. Meanwhile, the heat transfer deterioration zone moves away from the throat, which is beneficial to the thermal protection of the throat area.

Fig. 11b shows the temperature distribution of the regenerative coolant along the axial direction of the thrust chamber. Since the inlet of the cooling channel is located at the tail of the nozzle, the mainstream gas flows in the opposite direction to the coolant. The coolant temperature, therefore, increases in the axial direction of the thrust chamber and reaches saturation in the two-phase region, causing the temperature of the regenerative coolant to remain basically unchanged. The temperature rise of the regenerative coolant decreases due to the introduction of gas film cooling, and the temperature rise of the regenerative coolant decreases with the increase of the gas film cooling flow rate. When the gas film flow rate increases from 10% to 25%, the temperature rise decreases from 108 to 67 K. In addition, it is clear that in the vicinity of the inlet of the gas film, the temperature rise of the regenerative coolant is more gradual. This is because the majority of heat transferred from the mainstream gas to the wall is absorbed by the gas film for self-heating, while the heat transferred from the wall to the regenerative coolant is minimal.

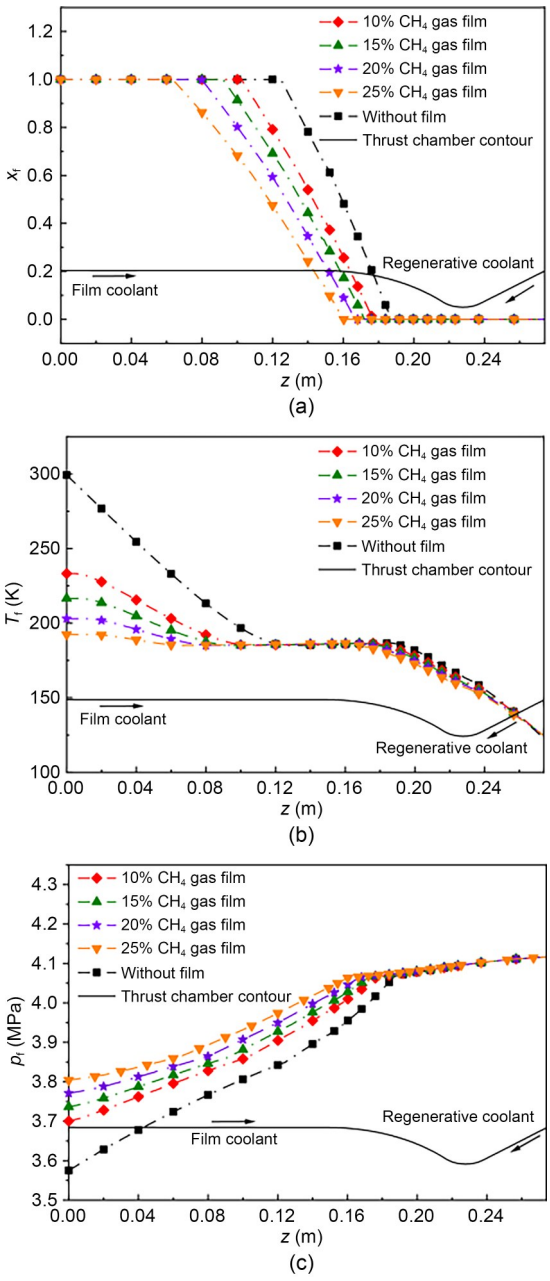

Fig. 11 Distribution of dryness x_f (a), temperature T_f (b), and pressure p_f (c) of the regenerative coolant

Fig. 11c shows the pressure distribution of the regenerative coolant along the axial direction of the thrust chamber. Because of frictional resistance, the pressure of the coolant decreases along the direction of flow. In the liquid-phase region, the curve changes more smoothly due to the slower flow of the regenerative coolant. After entering the two-phase region, the acceleration of the two-phase flow causes the curve to suddenly become steeper. The flow velocity in the gas-phase region is between that in the liquid-phase region

and that in the two-phases region, so the slope of the coolant pressure curve is also between the slopes in these two regions.

By comparing the curves in Fig. 11, it can be found that the change of the gas film mass flow rate has little influence on the parameters in the region near the entrance of the regenerative cooling channel. However, the total pressure drop of the regenerative coolant decreases from 0.54 to 0.32 MPa as the gas film flow rate increases, which greatly reduces pressure loss. This is because the influence of gas film cooling on the temperature of the regenerative coolant is mainly reflected in the gas-phase region. As the gas film mass flow rate increases, the temperature of the regenerative coolant and the flow velocity of the regenerative coolant in the gas-phase region decrease, reducing the overall pressure drop.

3.2.3 Gas-side wall temperature

Fig. 12 shows the distribution of the gas-side wall temperature (T_{wg}) along the axial direction of the thrust chamber. It can be seen from the figure that the variation trend of gas-side wall temperature of the gas film/regenerative composite cooling scheme is roughly the same as that of the regenerative cooling scheme. Along the regenerative coolant flow direction, the wall temperature rises first and then falls in the liquid-phase region, reaching an extreme value (T_{wg_LPV}) in the throat region. After entering the two-phase region, the gas-side wall temperature successively enters heat transfer enhancement (HTE) and heat transfer deterioration (HTD). In the HTE stage, the gas-side wall temperature is low and the variation range is small. After entering the HTD stage, the wall temperature rapidly increases to the maximum value (T_{wg_HTD}). The coolant absorbs heat as it flows through the cooling channels, leading to an increase in its dryness. Eventually, the coolant completely vaporizes, and the gaseous coolant provides thermal protection to the thrust chamber walls.

In the gas-phase region, there is a difference in the wall temperature variation curve between the single regenerative cooling scheme and the composite cooling scheme. In the single regenerative cooling scheme, due to the weaker heat transfer capability of the gaseous coolant, the wall temperature rises rapidly, and the maximum wall temperature reaches 700 K. However, in the composite cooling scheme, the cooling

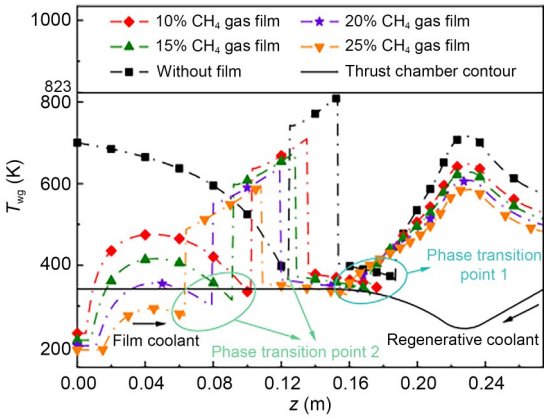

Fig. 12 Distribution of the wall temperature on the gas side at different mass flow rates

efficiency is higher near the introduction position, resulting in the wall temperature near the introduction point being approximately equal to the coolant temperature. Additionally, the introduction of film cooling at the head of the thrust chamber leads to a significant decrease in the wall temperature in the gas-phase region. When the methane film flow rate is 25%, the maximum wall temperature in the gas-phase region is only 595 K. From Fig. 12, it can be also observed that as the film flow rate increases, the higher the efficiency of film cooling at the same position, the lower the wall temperature of the thrust chamber.

Furthermore, it can be observed from Fig. 12 that the presence of film cooling leads to a reduction in the wall temperature of the thrust chamber in the two-phase region. As a result, the heat absorption by the coolant decreases, causing the position where the coolant enters the two-phase region to shift backwards with an increase in the length of the two-phase region. Additionally, a higher film flow rate results in a higher film cooling efficiency at the same position, leading to a lower wall temperature, reduced heat absorption by the coolant, and a further shift backwards of the position where the coolant enters the two-phase region, thereby increasing the length of the two-phase region. When the film flow rate is 25%, the maximum wall temperature (T_{wg_HTD}) in the two-phase region of the thrust chamber is only 595 K, which is 216 K lower compared to that in the single regenerative cooling scheme.

Furthermore, it can be observed from Fig. 12 that the wall temperature at the throat region of the thrust chamber decreases due to the introduction of film cooling at the head of the chamber. This is primarily because

the throat region is situated downstream of the film cooling introduction point and remains within the influence of the film cooling. As the film flow rate increases, the film cooling efficiency at the throat region also improves, resulting in a lower wall temperature. Specifically, when the film flow rate is 25%, the maximum wall temperature (T_{wg_LPV}) at the throat region of the thrust chamber is only 584 K, which represents a reduction of 129 K compared to the case of single regenerative cooling.

Based on the aforementioned analysis, it is evident that the introduction of film cooling has resulted in a substantial reduction in the gas-side wall temperature. The wall temperature of the thrust chamber is significantly below the material's limit temperature, thereby indicating a notable enhancement in the thermal protection capability of the chamber. Through the aforementioned analysis, the advantages of the gas film/regenerative composite cooling scheme in terms of thermal protection for the thrust chamber are preliminarily substantiated.

It is worth noting that there is a discrepancy in the calculation models for h_{co} between the two-phase region and the gas-phase region. This discrepancy results in a sudden discontinuity in h_{co} during the transition from the two-phase region to the gas-phase region, leading to an abrupt change in the wall temperature of the thrust chamber (Song et al., 2021). In reality, the temperature gradient of T_{wg} at the phase transition point does not change significantly, and there should be a transitional region within the abrupt change region. However, this model offers a significant advantage in terms of computational speed, and the calculated results provide a valuable reference for the preliminary design and analysis of thermal protection.

3.3 Influence of gas film introduction position on composite cooling performance

The influence of the gas film introduction position on the composite cooling performance is analyzed by comparing the variation of the gas-side temperature distribution. Based on the analysis in Section 3.2.2, the gas film with the same 20% mass flow rate is introduced from four positions: the head of the thrust chamber, the midpoint of the cylinder section, the right side of the cylinder section, and the midpoint of the convergent section. The specific schemes are shown in Fig. 13 and Table S2 of the ESM.

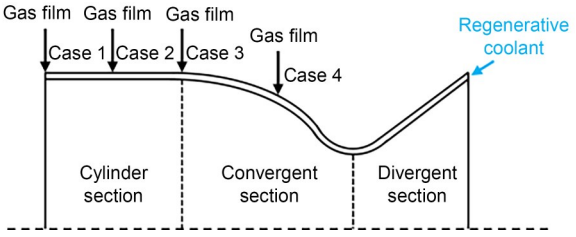

Fig. 13 Schematic diagram of the introduction positions of the gas film

3.3.1 Influence of the gas film introduction position on the gas-side wall temperature

Fig. 14 shows the gas-side wall temperature distribution for different introduction positions of the gas film. It can be seen in Fig. 14 that as the introduction position of the gas film is closer to the throat area, the position of T_{wg_HTD} will move towards the outlet of the regenerative cooling channel for cases 2–4.

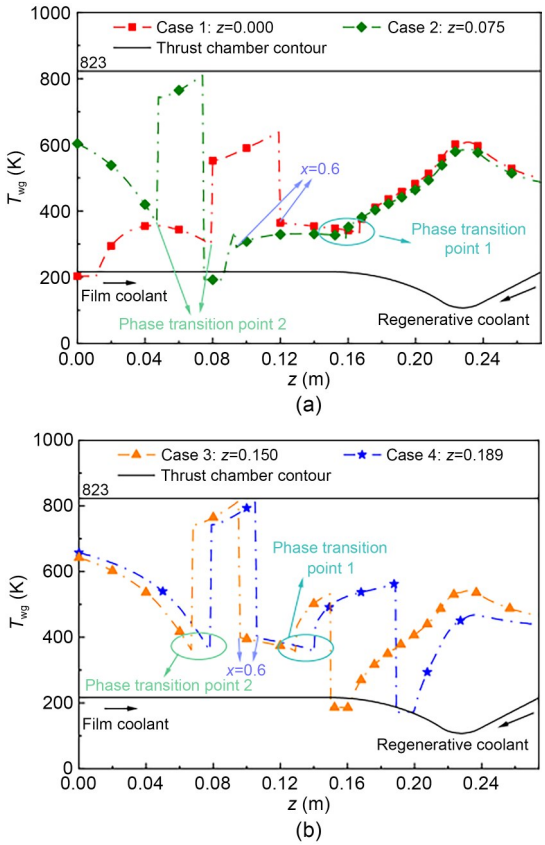

Fig. 14 Distribution of the wall temperature on the gas side at different introduction positions: (a) cases 1 and 2; (b) cases 3 and 4

However, for the internal physical processes corresponding to cases 1–4, case 3 and case 4 are more

similar, while there are slight differences between case 1 and case 2.

As shown in Fig. 14a, for case 2, the introduction of film cooling occurs just after the critical point where the dryness is 0.6. At this point, the film cooling region overlaps with the heat transfer enhancement region, resulting in a less pronounced cooling effect of film cooling. Additionally, in the upstream region of the film cooling introduction point, within the heat transfer deterioration region, the wall temperature remains relatively high due to the absence of film cooling assistance. On the other hand, for case 1, the film cooling introduction point is located at the top of the thrust chamber. Since this position is relatively close to both the heat transfer deterioration region and the gas-phase region, the overall wall temperature of the thrust chamber is lower compared to the other three cases. In case 1, T_{wg_HTD} is only 638.5 K, and the wall temperature is distributed more evenly along the axial direction, achieving an ideal cooling effect.

As shown in Fig. 14b, for cases 3 and 4, the film cooling introduction points are both located downstream of the phase transition point 1. Therefore, film cooling does not solve the thermal protection issue in the heat transfer deterioration region with the highest temperature reaching 810 K, only 13 K lower than the limit wall temperature of the material. It is observed that the closer the introduction position of gas film is to the throat, the lower the wall temperature of the area near the throat. However, in case 4, when the gas film is introduced from the midpoint of the convergent section, the wall temperature near the throat in the convergent segment increases sharply, which would have adverse effects on the wall structure and should be avoided.

To further explore the influence of the gas film introduction position on the gas-side wall temperature extremes of the heat transfer deterioration region and liquid-phase region (T_{wg_HTD} and T_{wg_LPV}), 41 introduction positions are selected and both wall temperature extremes under different introduction positions are calculated. The curves of the temperature extremes are illustrated in Fig. 15. In Fig. 15, the abscissa represents the introduction position of the gas film, while the ordinate represents the extreme gas-side wall temperature. The area near the throat is defined as the area between the axial coordinates z=0.200 and 0.255 m, i.e., the maximum wall temperature between z=0.200 and 0.255 m.

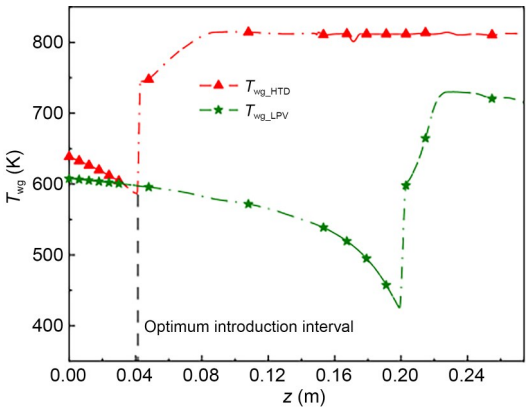

Fig. 15 Variation of the peak wall temperature on the gas side for different introduction positions

As the introduction position of the gas film moves away from the cooling channel outlet, T_{wg_LPV} and T_{wg_HTD} first decrease, then increase, and finally remain unchanged (Fig. 15). However, when the introduction position is between z=0.000 and 0.043 m, the curve has not yet turned and the peak wall temperature remains in the low range, always lower than 650 K. The extreme wall temperature near the throat also remains at about 600 K, which is far lower than the limit wall temperature of the material. The closer the introduction position to z=0.043 m, the lower the peak value of the gas-side wall temperature. Considering the heat transfer deterioration region and throat region comprehensively, it can be preliminarily determined that z= 0.043 m is the optimal introduction position at the gas film flow rate of 20%. The maximum gas-side wall temperature under these conditions is only 596 K, indicating that the gas film/regenerative composite cooling model has a good protection effect on the thrust chamber wall.

3.3.2 Influence of double-row hole position of gas film on gas-side wall temperature

The use of a multi-row jet is an effective approach for enhancing the cooling effectiveness, as demonstrated in (Li et al., 2019). Therefore, based on the analysis in Section 3.3.1, this study preliminarily explores the cooling effect of introducing the gas film into the cylinder section of the thrust chamber in two positions. Since it is difficult to enumerate the combination of double-row hole opening position and flow rate distribution, this study chooses three combination schemes for calculation and analysis. The gas film flow rate of both rows of holes is 10%. The first row

of holes is positioned at the head of the thrust chamber, while the second row of holes is positioned at the optimal introduction position described in Section 3.3.1, as well as the midpoint of the cylinder section and the right side of the cylinder section. To compare the differences between the double-row and single-row hole schemes, case 1 is compared with the aforementioned three cases (cases 5–7). The specific schemes are shown in Fig. 16 and Table S3 of the ESM.

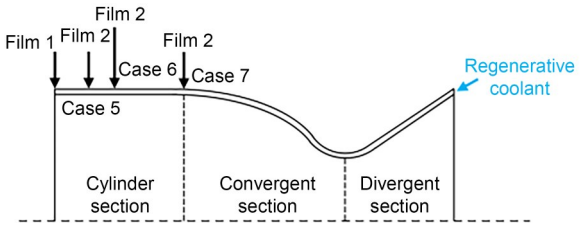

Fig. 16 Schematic diagram of the introduction positions of Film 1 and Film 2. Film 1 and Film 2 represent the first gas film and the second gas film, respectively

Fig. 17 shows the axial distribution of the gas-side wall temperature along the thrust chamber for four different schemes. Compared to case 1, the overall value of wall temperature decreases when the gas film is introduced from a double row of holes, demonstrating the superiority of the double row in gas film cooling. Comparing the curves of cases 5–7, little difference is observed in gas-side wall temperature distribution near the throat. However, case 5 has more obvious advantages in terms of the gas-side wall temperature distribution in the heat transfer deterioration region.

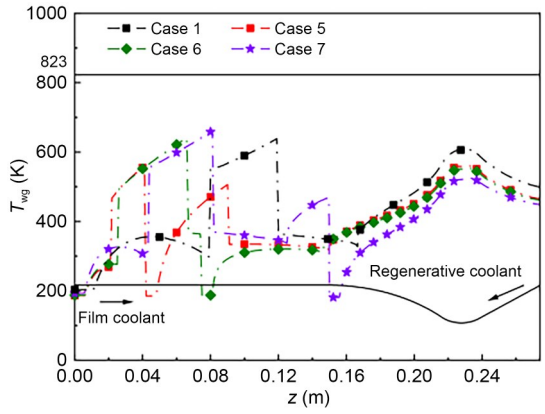

Fig. 17 Distribution of the gas-side wall temperature under the double row of holes

However, from the trend of the curve for the four cases, it can be observed that the curve for case 5 appears to deviate from the expected trend compared to cases 1, 6, and 7. Therefore, a detailed analysis will be conducted on the variation curve of case 5.

As shown in Fig. 18, in cases 1 and 5, the coolant undergoes phase transition starting from phase transition point 1. At this point, the coolant in close proximity to the wall undergoes vigorous boiling, leading to enhanced heat transfer. This results in an increase in the convective heat transfer coefficient and a slight decrease in the wall temperature of the thrust chamber. As the coolant continues to absorb heat, when the dryness reaches 0.6, the heat transfer between the wall and the liquid is disrupted by the low-thermal conductivity film layer. This leads to a heat transfer deterioration, causing a sudden increase in the wall temperature of the thrust chamber.

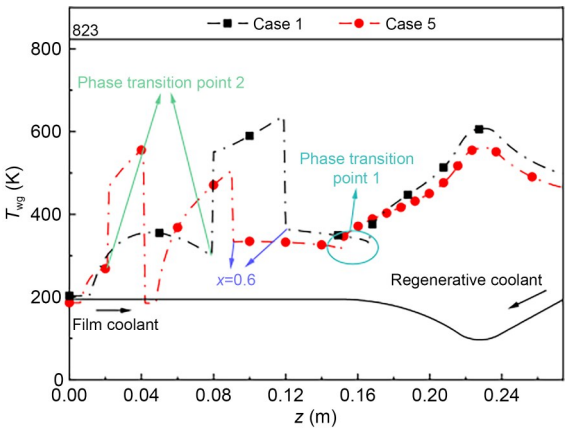

Fig. 18 Distribution of the wall temperature on the gas side of cases 1 and 5

In case 1, due to the film cooling introduction point positioned at the head of the thrust chamber, the coolant undergoes a phase transition to the gas phase at phase transition point 2 after passing through the heat deterioration zone.

In case 5, the film cooling introduction points are located at z=0.000 m and z=0.043 m. Moreover, the position of the heat deterioration region is shifted backwards compared to case 1. In this case, the film cooling introduction points are precisely within the heat deterioration region and the introduction of the film cooling causes a sudden decrease in the wall temperature of the thrust chamber (with a higher cooling efficiency at the film cooling introduction point). Subsequently, the wall temperature gradually increases. Additionally, due to the presence of film cooling, the

heat absorbed by the coolant is reduced, resulting in an elongation of the heat deterioration region. After passing through the film cooling introduction point, the coolant still maintains a dryness fraction between 0.6 and 1.0. At this point, the wall temperature increases again. However, because the heat deterioration region is closer to the head of the thrust chamber, it is also closer to the film cooling introduction position (the head of the thrust chamber). As a result, the maximum wall temperature in the heat deterioration region significantly decreases. As mentioned earlier, there is a sudden increase in wall temperature due to limitations of the model. However, overall, the advantage of the film cooling introduction point in case 5 leads to a lower wall temperature compared to other cases.

Subsequently, we can consider reducing the distance between the two rows of holes or changing the introduction position of the first row of holes to further explore how to efficiently organize the double row of holes in the gas film/regenerative composite cooling scheme.

4 Conclusions

In this study, a gas film/regenerative composite cooling calculation model for the thrust chamber of the liquid oxygen/methane engine is established and a heat transfer analysis is conducted based on the EEC engine at 75% RPL. The heat transfer characteristic parameters (e.g., coolant temperature rise, pressure drop, and gas-side wall temperature) are also calculated and analyzed. This study explores the influence of the gas film flow rate, gas film introduction position, and double-row hole introduction position on the gas-side wall temperature. The following conclusions can be drawn:

(1) The gas film/regenerative composite cooling model is established in this study based on the Grisson gas film cooling efficiency formula and the one-dimensional regenerative cooling model. The one-dimensional composite cooling heat transfer model offers the advantages of low computational cost in calculation and is accurate enough to be used as a preliminary design tool. Compared with the experimental results, the temperature rise error of coolant is less than 10%.

(2) Increasing the gas film flow rate strengthens the cooling effect and reduces the amount of heat transferred to the regenerative coolant. The phase transition point of the regenerative coolant moves towards the outlet of the cooling channel, causing the temperature to rise, the pressure drop to decrease, and the gas-side wall temperature to decrease accordingly. At a gas film flow rate of 25%, the peak wall temperature is only 595 K, which is far lower than the material temperature limit.

(3) The optimal introduction position is achieved when the gas film is introduced by a single row of holes, allowing the gas-side wall temperature to be distributed more evenly and lowering the peak value. At a gas film flow rate of 20%, the ideal introduction position is z=0.043 m and the peak wall temperature is 596 K.

It is worth noting that the conclusions mentioned above are derived from specific simulation calculations conducted on a particular thrust chamber under specific operating conditions. Therefore, these conclusions cannot be directly applied to other specific cases. However, the above heat transfer calculation model can be applied to conduct similar heat transfer studies on a thrust chamber with gas film/regenerative composite cooling.

Acknowledgments

This work is supported by the National Science Fund Project (No. 2019-JCJQ-ZQ-019) and the Innovative Research Group Project of National Natural Science Foundation of China (No. T2221002).

Author contributions

Xinlin LIU and Jun SUN designed the research. Xinlin LIU and Jun SUN processed the corresponding data. Xinlin LIU and Jun SUN wrote the first draft of the manuscript. Zhuohang JIANG and Qinglian LI helped to organize the manuscript. Peng CHENG and Jie SONG revised and edited the final version.

Conflict of interest

Xinlin LIU, Jun SUN, Zhuohang JIANG, Qinglian LI, Peng CHENG, and Jie SONG declare that they have no conflict of interest.

References

Ali MS, Anwar Z, Mujtaba MA, et al., 2021. Two-phase frictional pressure drop with pure refrigerants in vertical mini/micro-channels. *Case Studies in Thermal Engineering*, 23:100824. https://doi.org/10.1016/j.csite.2020.100824

Bertsch SS, Groll EA, Garimella SV, 2008. Refrigerant flow boiling heat transfer in parallel microchannels as a function of local vapor quality. *International Journal of Heat*

and Mass Transfer, 51(19-20):4775-4787. https://doi.org/10.1016/j.ijheatmasstransfer.2008.01.026

Cary AM, Hefner JN, 1972. Film-cooling effectiveness and skin friction in hypersonic turbulent flow. *AIAA Journal*, 10(9):1188-1193. https://doi.org/10.2514/3.50348

Dannenberg RE, 1962. Helium Film Cooling on a Hemisphere at a Mach Number of 10. Technical Report No. NASA TN D-1550, NASA Ames Research Center, Moffett Field, USA.

Gao XF, Zhang JW, Sun B, et al., 2018. Study on optimal gas film parameters of near-injection region in thrust chamber. *Journal of Rocket Propulsion*, 44(2):10-17 (in Chinese).

Goldstein RJ, 1971. Film cooling. *Advances in Heat Transfer*, 7:321-379. https://doi.org/10.1016/S0065-2717(08)70020-0

Goldstein RJ, Eckert ERG, Tsou FK, et al., 1966. Film cooling with air and helium injection through a rearward-facingslot into a supersonic air flow. *AIAA Journal*, 4(6):981-985. https://doi.org/10.2514/3.3591

Gradl PR, Protz CS, 2020. Technology advancements for channel wall nozzle manufacturing in liquid rocket engines. *Acta Astronautica*, 174:148-158. https://doi.org/10.1016/j.actaastro.2020.04.067

Gururatana S, Prapainop R, Chuepeng S, et al., 2021. Development of heat transfer performance in tubular heat exchanger with improved NACA0024 vortex generator. *Case Studies in Thermal Engineering*, 26:101166. https://doi.org/10.1016/j.csite.2021.101166

Hao JH, Chen Q, Li X, et al., 2021. A correction factor-based general thermal resistance formula for heat exchanger design and performance analysis. *Journal of Thermal Science*, 30(3):892-901. https://doi.org/10.1007/s11630-021-1369-8

Heufer KA, Olivier H, 2006. Film cooling of an inclined flat plane in hypersonic flow. The 14th AIAA/AHI Space Planes and Hypersonic Systems and Technologies Conference, p.1-14. https://doi.org/10.2514/6.2006-8067

Hong Y, Liu ZY, Silvestri S, et al., 2019. An experimental and modelling study of heat loads on a subscale methane rocket motor. *Acta Astronautica*, 164:112-120. https://doi.org/10.1016/j.actaastro.2019.07.011

Howard FG, Srokowski AJ, 1977. Cooling effectiveness of slot injection into a turbulent boundary layer. *AIAA Journal*, 15(9):1366-1368. https://doi.org/10.2514/3.7433

Huzel DK, Huang DH, 1992. Modern Engineering for Design of Liquid-Propellant Rocket Engines. American Institute of Aeronautics and Astronautics, Washington, USA, p.147.

Jagannathan R, Elliott M, Johansen C, et al., 2018. Study of heat transfer with surface treatment in pre-coolers for aeroengine applications. *Case Studies in Thermal Engineering*, 12:742-748. https://doi.org/10.1016/j.csite.2018.10.002

Kanda T, Masuya G, Ono F, et al., 1994. Effect of film cooling/regenerative cooling on scramjet engine performances. *Journal of Propulsion and Power*, 10(5):618-624. https://doi.org/10.2514/3.23771

Keller MA, Kloker MJ, 2017. Direct numerical simulation of foreign-gas film cooling in supersonic boundary-layer flow. *AIAA Journal*, 55(1):99-111. https://doi.org/10.2514/1.J055115

Keller MA, Kloker MJ, Olivier H, 2015. Influence of cooling-gas properties on film-cooling effectiveness in supersonic flow. *Journal of Spacecraft and Rockets*, 52(5):1443-1455. https://doi.org/10.2514/1.A33203

Konopka M, Meinke M, Schröder W, 2012. Large-eddy simulation of shock/cooling-film interaction. *AIAA Journal*, 50(10):2102-2114. https://doi.org/10.2514/1.J051405

Li GC, Gao ZY, Zhang W, et al., 2019. Effects of combination of forward jet and backward jet with two rows of holes on film cooling. *Journal of Propulsion Technology*, 40(3):643-652 (in Chinese). https://doi.org/10.13675/j.cnki.tjjs.180225

Li MC, Wei SS, Huang CH, et al., 2022. Experimental and numerical investigation of swirling H_2O_2 and polypropylene hybrid rocket motor with regenerative cooling. *Acta Astronautica*, 190:283-298. https://doi.org/10.1016/j.actaastro.2021.09.026

Liang T, Song J, Li QL, et al., 2021. System scheme design of electric expander cycle for LOX/LCH4 variable thrust liquid rocket engine. *Acta Astronautica*, 186:451-464. https://doi.org/10.1016/j.actaastro.2021.06.015

Liang T, Xu WW, Ye W, et al., 2023. Study on the heat transfer characteristics of a plate-fin-typed precooler considering cooling fluid phase change. *Case Studies in Thermal Engineering*, 47:103073. https://doi.org/10.1016/j.csite.2023.103073

Lushchik VG, Yakubenko AE, 2001. Tangential-slot film cooling on a plate in supersonic flow. Comparison of calculation and experiment. *Fluid Dynamics*, 36(6):926-933. https://doi.org/10.1023/A:1017914710250

Metzger DE, Carper HJ, Swank LR, 1968. Heat transfer with film cooling near nontangential injection slots. *Journal of Engineering for Power*, 90(2):157-162. https://doi.org/10.1115/1.3609155

Miao HY, Wang ZW, Niu YB, 2020a. Performance analysis of cooling system based on improved supercritical CO_2 Brayton cycle for scramjet. *Applied Thermal Engineering*, 167:114774. https://doi.org/10.1016/j.applthermaleng.2019.114774

Miao HY, Wang ZW, Niu YB, 2020b. Key issues and cooling performance comparison of different closed Brayton cycle based cooling systems for scramjet. *Applied Thermal Engineering*, 179:115751. https://doi.org/10.1016/j.applthermaleng.2020.115751

Peng W, Jiang PX, 2009. Influence of shock waves on supersonic film cooling. *Journal of Spacecraft and Rockets*, 46(1):67-73. https://doi.org/10.2514/1.38458

Peng W, Sun XK, Jiang PX, et al., 2017. Effect of continuous or discrete shock wave generators on supersonic film cooling. *International Journal of Heat and Mass Transfer*, 108:770-783.

https://doi.org/10.1016/j.ijheatmasstransfer.2016.12.044

Perakis N, Haidn OJ, 2020. Wall heat transfer prediction in CH_4/O_2 and H_2/O_2 rocket thrust chambers using a non-adiabatic flamelet model. *Acta Astronautica*, 174:254-269. https://doi.org/10.1016/j.actaastro.2020.05.008

Phu NM, Hap NV, 2020. Influence of inlet water temperature on heat transfer and pressure drop of dehumidifying air coil using analytical and experimental methods. *Case Studies in Thermal Engineering*, 18:100581. https://doi.org/10.1016/j.csite.2019.100581

Pizzarelli M, 2021. Overview and analysis of the experimentally measured throat heat transfer in liquid rocket engine thrust chambers. *Acta Astronautica*, 184:46-58. https://doi.org/10.1016/j.actaastro.2021.03.028

Pizzarelli M, Nasuti F, Onofri M, 2014. Effect of cooling channel aspect ratio on rocket thermal behavior. *Journal of Thermophysics and Heat Transfer*, 28(3):410-416. https://doi.org/10.2514/1.T4299

Ruan B, Huang SZ, Meng H, et al., 2017. Transient responses of turbulent heat transfer of cryogenic methane at supercritical pressures. *International Journal of Heat and Mass Transfer*, 109:326-335. https://doi.org/10.1016/j.ijheatmasstransfer.2017.02.006

Song J, Liang T, Li QL, et al., 2021. Study on the heat transfer characteristics of regenerative cooling for LOX/LCH4 variable thrust rocket engine. *Case Studies in Thermal Engineering*, 28:101664. https://doi.org/10.1016/j.csite.2021.101664

Sun B, Zhang JW, 2016. Thermal Protection Technology of Rocket Engine. Beihang University Press, Beijing, China, p.84-112 (in Chinese).

Sun B, Yang W, Zheng LM, et al., 2013. Numerical simulation of liquid film and regenerative cooling in a rocket combustor. *Journal of Aerospace Power*, 28(6):1357-1363 (in Chinese). https://doi.org/10.13224/j.cnki.jasp.2013.06.008

Takita K, Masuya G, 2000. Effects of combustion and shock impingement on supersonic film cooling by hydrogen. *AIAA Journal*, 38(10):1899-1906. https://doi.org/10.2514/2.843

Thome JR, Consolini L, 2010. Mechanisms of boiling in microchannels: critical assessment. *Heat Transfer Engineering*, 31(4):288-297. https://doi.org/10.1080/01457630903312049

Trejo A, Garcia C, Choudhuri A, 2016. Experimental investigation of transient forced convection of liquid methane in a channel at high heat flux conditions. *Experimental Heat Transfer*, 29(1):97-112. https://doi.org/10.1080/08916152.2014.945052

Wan H, Yuan B, Qin F, et al., 2020. Numerical simulation of composite cooling of RBCC ejector rocket using gradient micro-channels. *Journal of Engineering Thermophysics*, 41(5):1179-1185 (in Chinese).

Waxenegger-Wilfing GW, Dresia K, Deeken JC, et al., 2020. Heat transfer prediction for methane in regenerative cooling channels with neural networks. *Journal of Thermophysics and Heat Transfer*, 34(2):347-357. https://doi.org/10.2514/1.T5865

Yang W, Sun B, 2013. Numerical simulation of liquid film and regenerative cooling in a liquid rocket. *Applied Thermal Engineering*, 54(2):460-469. https://doi.org/10.1016/j.applthermaleng.2013.02.021

Yang XB, Badcock KJ, Richards BE, et al., 2003. Numerical simulation of film cooling in hypersonic flows. The 36th AIAA Thermophysics Conference, p.1-7. https://doi.org/10.2514/6.2003-3631

Yang XB, Badcock KJ, Richards BE, et al., 2005. A numerical study of hypersonic turbulent film cooling. The 43rd AIAA Aerospace Sciences Meeting and Exhibit, p.1-15. https://doi.org/10.2514/6.2005-386

Yu WL, Zhou WX, Jia ZJ, et al., 2022. Characteristics of scramjet regenerative cooling with endothermic chemical reactions. *Acta Astronautica*, 195:1-11. https://doi.org/10.1016/j.actaastro.2022.02.025

Zeng M, Liu W, Zou JJ, 2016. Fundamentals of Aerodynamics. Science Press, Beijing, China, p.203-214 (in Chinese).

Zhang BC, Li QL, Wang Y, et al., 2020. Experimental investigation of nitrogen flow boiling heat transfer in a single mini-channel. *Journal of Zhejiang University-SCIENCE A (Applied Physics & Engineering)*, 21(2):147-166. https://doi.org/10.1631/jzus.A1900468

Zhang HW, He YL, Tao WQ, 2007. Numerical study of film and regenerative cooling in a thrust chamber at high pressure. *Numerical Heat Transfer, Part A: Applications*, 52(11):991-1007. https://doi.org/10.1080/10407780701364379

Zhang M, Sun B, 2020. Effect of artificial roughness on flow and heat transfer of transcritical methane. *International Journal of Thermal Sciences*, 158:106528. https://doi.org/10.1016/j.ijthermalsci.2020.106528

Zhang SL, Qin J, Xie KL, et al., 2016. Thermal behavior inside scramjet cooling channels at different channel aspect ratios. *Journal of Propulsion and Power*, 32(1):57-70. https://doi.org/10.2514/1.B35563

Zhang YL, 1984. State-space analysis of the dynamic characteristics of a variable thrust liquid propellant rocket engine. *Acta Astronautica*, 11(7-8):535-541. https://doi.org/10.1016/0094-5765(84)90093-6

Zhang ZL, Zhang MZ, Zhou LX, 2016. Liquid Rocket Engine Thermal Protection. National Defense Industry Press, Beijing, China (in Chinese).

Zhou C, Yu NJ, Wang J, et al., 2021. Analysis of dynamic characteristics and sensitivity of hydrogen-oxygen expansion cycle rocket engine system. *Acta Astronautica*, 189:624-637. https://doi.org/10.1016/j.actaastro.2021.08.046

Zhu NC, Liu GD, 2009. Liquid Rocket Engine Design. China Aerospace Press, Beijing, China, p.545 (in Chinese).

Zuo JY, Zhang SL, Qin J, et al., 2018. Performance evaluation of regenerative cooling/film cooling for hydrocarbon fueled scramjet engine. *Acta Astronautica*, 148:57-68. https://doi.org/10.1016/j.actaastro.2018.04.037

Electronic supplementary materials

Sections S1–S8, Fig. S1, Tables S1–S3